

# Melt Electrowriting of Amphiphilic Physically Crosslinked Segmented Copolymers

Ezgi Bakirci, Andreas Frank, Simon Gumbel, Paul F. Otto, Eva Fürsattel, Ingrid Tessmer, Hans-Werner Schmidt,\* and Paul D. Dalton\*

Various (AB)<sub>n</sub> and (ABAC)<sub>n</sub> segmented copolymers with hydrophilic and hydrophobic segments are processed via melt electrowriting (MEW). Two different (AB)<sub>n</sub> segmented copolymers composed of bisurea segments and hydrophobic poly(dimethyl siloxane) (PDMS) or hydrophilic poly(propylene oxide)-poly(ethylene oxide)-poly(propylene oxide) (PPO-PEG-PPO) segments, while the amphiphilic (ABAC)<sub>n</sub> segmented copolymers consist of bisurea segments in the combination of hydrophobic PDMS segments and hydrophilic PPO-PEG-PPO segments with different ratios, are explored. All copolymer compositions are processed using the same conditions, including nozzle temperature, applied voltage, and collector distance, while changes in applied pressure and collector speed altered the fiber diameter in the range of 7 and 60 μm. All copolymers showed excellent processability with MEW, well-controlled fiber stacking, and inter-layer bonding. Notably, the surfaces of all four copolymer fibers are very smooth when visualized using scanning electron microscopy. However, the fibers show different roughness demonstrated with atomic force microscopy. The non-cytotoxic copolymers increased L929 fibroblast attachment with increasing PDMS content while the different copolymer compositions result in a spectrum of physical properties.

## 1. Introduction

Additive manufacturing (AM) technologies have been used for different applications including soft robotics,<sup>[1]</sup> sensors,<sup>[2]</sup> biomaterials,<sup>[3,4]</sup> and tissue engineering.<sup>[4]</sup> AM, often referred to as 3D printing, is based on layer-by-layer fabrication principles that are employed by a spectrum of different technologies.<sup>[5]</sup> Melt electrowriting (MEW) is one such AM technology that uses an applied electric field to produce fine fiber diameters,<sup>[6]</sup> typically much smaller than 100 μm,<sup>[7]</sup> and 820 nm at their smallest to date.<sup>[8]</sup> The high viscosity of polymer melts assists in the reduction in fiber diameter without jet breakup<sup>[6]</sup> and computer-aided control of the collector direct-writes the desired pattern according to G-codes.<sup>[9]</sup>

While different polymers can be processed via MEW, poly( $\epsilon$ -caprolactone) (PCL) is the benchmark polymer due to its low melting point (60 °C) and slow thermal/hydrolytic degradation.<sup>[10]</sup> Beyond PCL, other polymers processed with MEW

include poly(vinylidene difluoride),<sup>[11]</sup> polypropylene,<sup>[12]</sup> poly(L-lactide-co- $\epsilon$ -CL-co-acryloyl carbonate),<sup>[13]</sup> poly(L-lactide-co-caprolactone),<sup>[14]</sup> poly(2-ethyl-2-oxazoline),<sup>[15]</sup> poly(urea-siloxane)<sup>[16]</sup> and poly(urea-ethylene glycol).<sup>[17]</sup> The majority of polymers processed to date are hydrophobic, which absorb proteins that influence cell adhesion.<sup>[18]</sup>

Hydrophilic polymers can reduce cell adhesion,<sup>[19]</sup> recently more and more are available for MEW, which, in turn, aids certain biomedical devices to improve their function.<sup>[20]</sup> The improved hydrophilic properties can thus result in a significant enhancement in the biocompatibility and functionality of the materials.<sup>[21]</sup> Within biofabrication, where soluble properties have utility in the formation of perfusable channels, the polymer may need to be water-soluble over time,<sup>[22,23]</sup> or on-demand.<sup>[24]</sup> Additionally, for any application that involves contact with cells, the polymers should be cytocompatible.<sup>[25]</sup>


Electrohydrodynamically stabilized jets of aqueous-based polymer and macromer solutions have been previously reported,<sup>[26,27]</sup> with post-crosslinking required to achieve a hydrogel fiber. When processing via MEW, however, hydrogel fibers are made by printing a melt and then swelling in aqueous media.<sup>[7]</sup> Since the preprinting period for MEW requires extrusion through a nozzle, non-crosslinked melts that crosslink after deposition has been developed and reported. There are

E. Bakirci, P. F. Otto, P. D. Dalton  
 Department for Functional Materials in Medicine and Dentistry and  
 Bavarian Polymer (BPI) Institute  
 University Würzburg  
 Pleicherwall 2, Würzburg 97070, Germany  
 E-mail: pdalton@uoregon.edu

A. Frank, S. Gumbel, E. Fürsattel, H.-W. Schmidt  
 Macromolecular Chemistry and Bavarian Polymer Institute (BPI)  
 University of Bayreuth  
 Universitätsstraße 30, Bayreuth 95440, Germany  
 E-mail: hans-werner.schmidt@uni-bayreuth.de

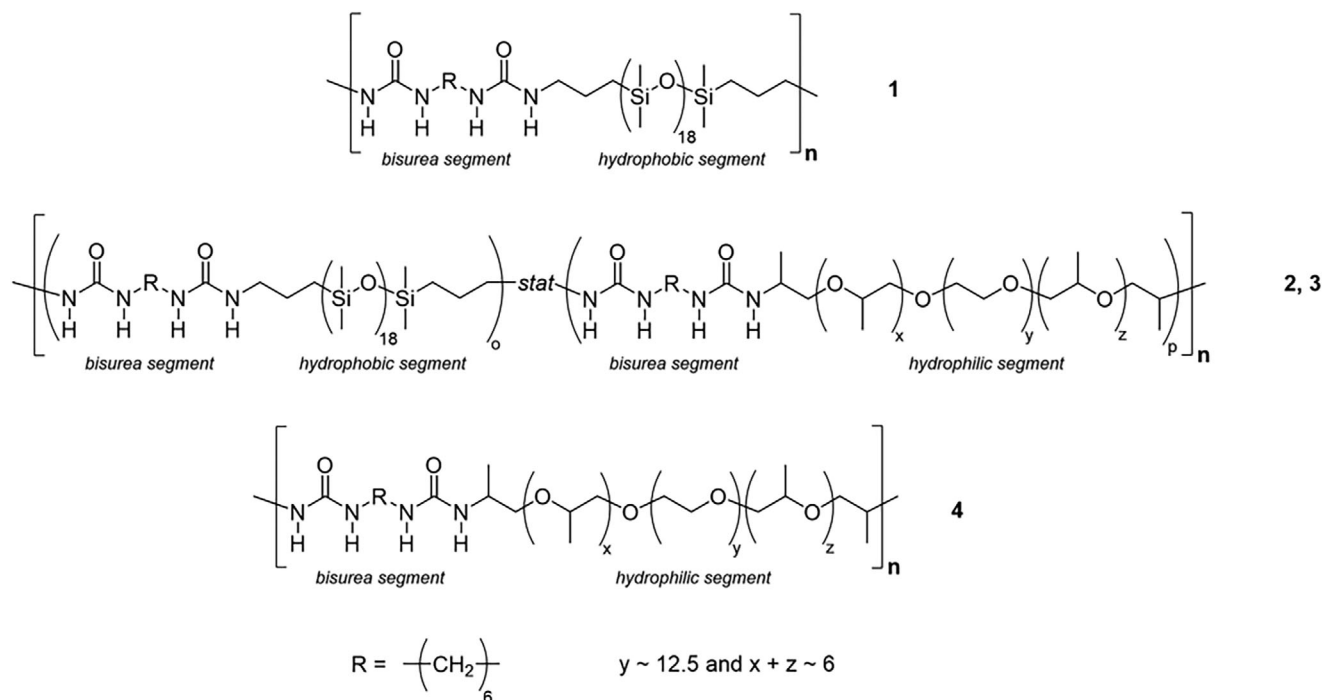
I. Tessmer  
 Rudolf-Virchow Center for Integrative and Translational Bioimaging  
 University of Würzburg  
 Josef-Schneider-Straße 2, Würzburg 97080, Germany

P. D. Dalton  
 Phil and Penny Knight Campus to Accelerate Scientific Impact  
 University of Oregon  
 1505 Franklin Blvd, Eugene, OR 90403, USA

 The ORCID identification number(s) for the author(s) of this article can be found under <https://doi.org/10.1002/macp.202100259>

© 2021 The Authors. Macromolecular Chemistry and Physics published by Wiley-VCH GmbH. This is an open access article under the terms of the Creative Commons Attribution License, which permits use, distribution and reproduction in any medium, provided the original work is properly cited.

DOI: 10.1002/macp.202100259



| Copolymer No. | Segment content (wt.%) |      |             |
|---------------|------------------------|------|-------------|
|               | Bisurea                | PDMS | PPO-PEG-PPO |
| 1             | 12                     | 88   | 0           |
| 2             | 13                     | 80   | 7           |
| 3             | 15                     | 53   | 32          |
| 4             | 19                     | 0    | 81          |

**Figure 1.** Chemical structures of the  $(AB)_n$  segmented bisurea copolymer **1** and **4**, and the  $(ABAC)_n$  segmented copolymers **2** and **3**. In all cases, the bisurea segments contain a hexamethylene unit. The copolymers differ in the content of the different segments as listed in the table.

several ways to achieve this crosslinking, including via UV-light,<sup>[13]</sup> Diels–Alder chemistry,<sup>[15]</sup> or using physical crosslinking such as reported with  $(AB)_n$  segmented copolymers.<sup>[17]</sup> The  $(AB)_n$  segmented copolymers belong to the class of physically crosslinked hydrogels. These copolymers are based on reversible, non-covalent crosslinks formed by hydrogen bonding, which allows the processing from the melt.<sup>[28]</sup> The processability of  $(AB)_n$  segmented copolymers with MEW provides unique properties due to high-resolution printing and design flexibility, which makes them interesting for optics,<sup>[29]</sup> microfluidics,<sup>[30]</sup> flexible electronic devices,<sup>[31]</sup> and soft network composites<sup>[32]</sup> in materials science and soft robotics. This study investigated the MEW processability of four different  $(AB)_n$  and  $(ABAC)_n$  segmented copolymers combined of bisurea, hydrophobic poly(dimethyl siloxane) (PDMS), and hydrophilic

poly(propylene oxide)-poly(ethylene oxide)-poly(propylene oxide) (PPO-PEG-PPO) segments (**Figure 1**). These copolymers have adjustable hydrophilic properties depending on their content of PPO-PEG-PPO segments. Copolymer **1** is hydrophobic due to the PDMS segments, whereas copolymer **4** is hydrophilic due to the PPO-PEG-PPO segments. Copolymers **2** and **3**, however, have different hydrophobic and hydrophilic properties depending on PDMS and PPO-PEG-PPO segment contents.  $(AB)_n$  and  $(ABAC)_n$  segmented copolymers are ideally suited for MEW due to their physical crosslinks reversibly disassemble and assemble upon heating and cooling, respectively. For all copolymers, MEW processing conditions such as molten polymer temperature, applied pressure, voltage, tip to collector distance, and collector speed<sup>[28,29]</sup> were systematically investigated, and the fiber diameter was correlated with the pressure and collector

speed. The copolymers used in this study have unique properties compared to polymers, which have been already processed with MEW including i) thermally reversibility, ii) a highly smooth surface, iii) transparency, iv) strong inter-layer bonding between the fibers, and v) adjustable hydrophilic and hydrophobic behavior. The morphology, mechanical properties, cytotoxicity, and cell adhesion behavior of the copolymers and the MEW scaffolds were examined.

## 2. Results and Discussion

### 2.1. Copolymer Properties

The  $(AB)_n$  segmented copolymers are composed of bisurea segments and hydrophobic PDMS or hydrophilic PPO-PEG-PPO segments (Figure 1). Furthermore, the  $(ABAC)_n$  segmented copolymers contain all three segments: besides bisurea, both hydrophobic, and hydrophilic segments are now incorporated in the same polymer chain by varying compositions. The bisurea segment is responsible for the thermoreversible physical crosslinking of the copolymer chains due to the formation of strong bidental hydrogen bonds. The hydrophobic PDMS segments provide mechanical stability, while water uptake is governed by the hydrophilic PPO-PEG-PPO segments. The hydrophilicity and thus water uptake can be adjusted by varying the ratio of PDMS to PPO-PEG-PPO segments. Extensive details on the polymer synthesis and resulting bulk properties can be found elsewhere.<sup>[33]</sup>

### 2.2. MEW Processing

For the successful printing of MEW constructs, the polymer melt viscosity at the processing temperature is an important parameter. Thus, the melt viscosity should be low enough to allow extrusion through the fine nozzle at pressures governed by the experimental setup. As shown in previous studies on similar  $(AB)_n$  segmented copolymers,<sup>[16,17]</sup> complex melt viscosities are comparable to viscosities obtained by rotational measurements, thus comply with the Cox/Merz relationship. The complex melt viscosity ( $\eta^*$ ) for the copolymers 1 to 4 upon cooling from the melt was measured at the MEW processing temperature of 100 °C by oscillatory shear rheology and are depicted in Figure 2. At this temperature,  $\eta^*$  was found in the range between 40 and 500 Pa s, thus suitable for MEW in the existing MEW printer configuration. Upon heating, the physical crosslinks of the urea bonds disaggregate into a viscous melt and, when cooled, the viscosity curves show a sudden increase between 70 and 40 °C. This increase in viscosity is caused by the distinct hydrogen bond re-aggregation typical for hexamethylene urea groups. At room temperature for all segmented copolymers, the  $\eta^*$  is around three orders of magnitude higher compared to the values in the melt. Thus, a fast solidification of the printed MEW constructs is expected.

While MEW is a multi-parametric manufacturing technology, which is typically optimized for each polymer, here we aimed to process the four different copolymers under similar conditions. When using identical processing parameters — applied pressure

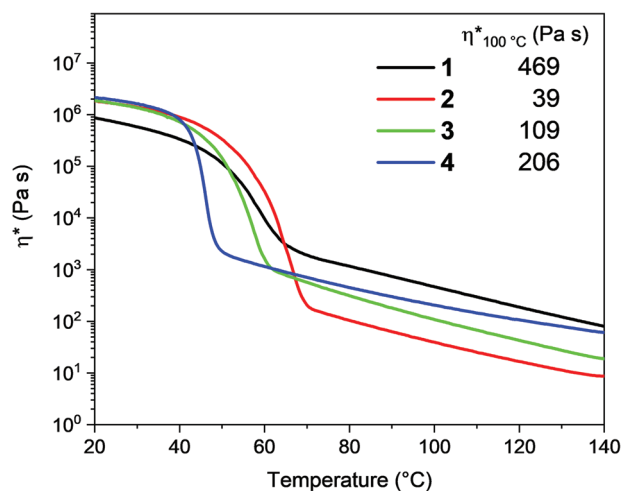


**Figure 2.** Complex melt viscosity ( $\eta^*$ ) versus temperature, shown are the first cooling curves of copolymers 1, 2, 3, and 4. Values of  $\eta^*$  at the MEW processing temperature of 100 °C are listed also in the plot. (Conditions: oscillating shear rheology utilizing a plate-plate geometry (25 mm) at 1 Hz with a cooling rate of 2 K min<sup>-1</sup>).

and collector speed included — notably different jet behaviors resulted for copolymers 1 to 4 (Figure 3 and Video S1, Supporting Information). The critical translational speed (CTS) is when the collector speed matches the molten jet speed and is determined experimentally as a straight line<sup>[34]</sup> of the polymer jet towards the collector as seen for copolymer 3 (Figure 3C). Increasing the collector speed beyond the CTS increases the lag of the jet, as observed for copolymer 1 and 2 in Figure 3A,B, and affects the accuracy of the printed constructs.<sup>[35,36]</sup> For copolymer 4, the jet speed is slightly faster than the collector speed and a pronounced heel appears, where the jet moves ahead of the nozzle (black arrow; Figure 3D).

Parameters such as applied voltage (3 kV), collector distance (2.2 mm) and melt processing temperature (100 °C) were kept constant for all four copolymers. The influence of the applied pressure and collector speed was investigated and is shown in Figure 3E. The thinnest fiber diameter,  $7.6 \pm 3.0 \mu\text{m}$ , was achieved using 2800 mm min<sup>-1</sup> collector speed and 1 bar for copolymer 1. The thickest fiber diameter was obtained using a low collector speed of 500 mm min<sup>-1</sup> and 1 bar, which results in  $59.0 \pm 12.5 \mu\text{m}$  for copolymer 4. In general, and in line with previous studies for other copolymers,<sup>[37]</sup> the fiber diameter decreases with increasing collector speed due to the mechanical stretching of the jet. An increase in the pressure also resulted in a thicker fiber diameter due to increased mass in the jet.

The fiber diameter did not significantly reduce at speeds greater than 1500 mm min<sup>-1</sup> for both applied pressures of 0.5 and 1 bar. The fiber diameter at 1 bar resulted in fiber pulsing with long beading<sup>[34]</sup> and substantially varied compared to 0.5 bar. Comparing the four copolymers, the viscosity and probably the ratio of PPO-PEG-PPO segments in the copolymer appeared to affect the fiber diameter, with copolymer 4 having the thickest fiber diameter. The CTS of copolymer 4 was also higher than the CTS of the other copolymers. All copolymers generally printed well, and defined scaffolds could be readily fabricated. The stacking behavior of the fibers was examined using

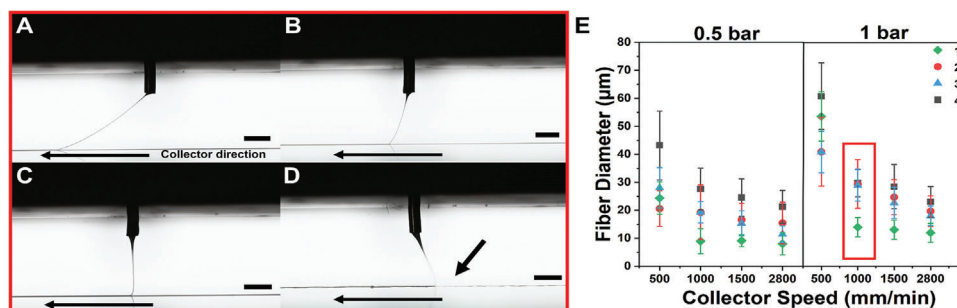


**Figure 3.** Jet behavior of four different copolymers using the same processing parameter ( $100\text{ }^{\circ}\text{C}$ ,  $1000\text{ mm min}^{-1}$ ,  $1\text{ bar}$ , and  $3\text{ kV}$ , see red box on the graph). Copolymers **1** A), B) **2**, C) **3** have a typical jet lag which can be seen when the collector speed is faster or equal to CTS and the fibers are straight, however, copolymer D) **4** has a pronounced “heel” typical when the collector speed is lower than the CTS, and it advances in front of the nozzle and the fibers are non-linear (scale bar:  $1\text{ mm}$ ) (see Video S1, Supporting Information). E) Effect of pressure and collector speed on the fiber diameter for the copolymers **1** to **4** at  $100\text{ }^{\circ}\text{C}$  of melt processing temperature,  $2.2\text{ mm}$  of collector distance, and  $3\text{ kV}$  of applied voltage.

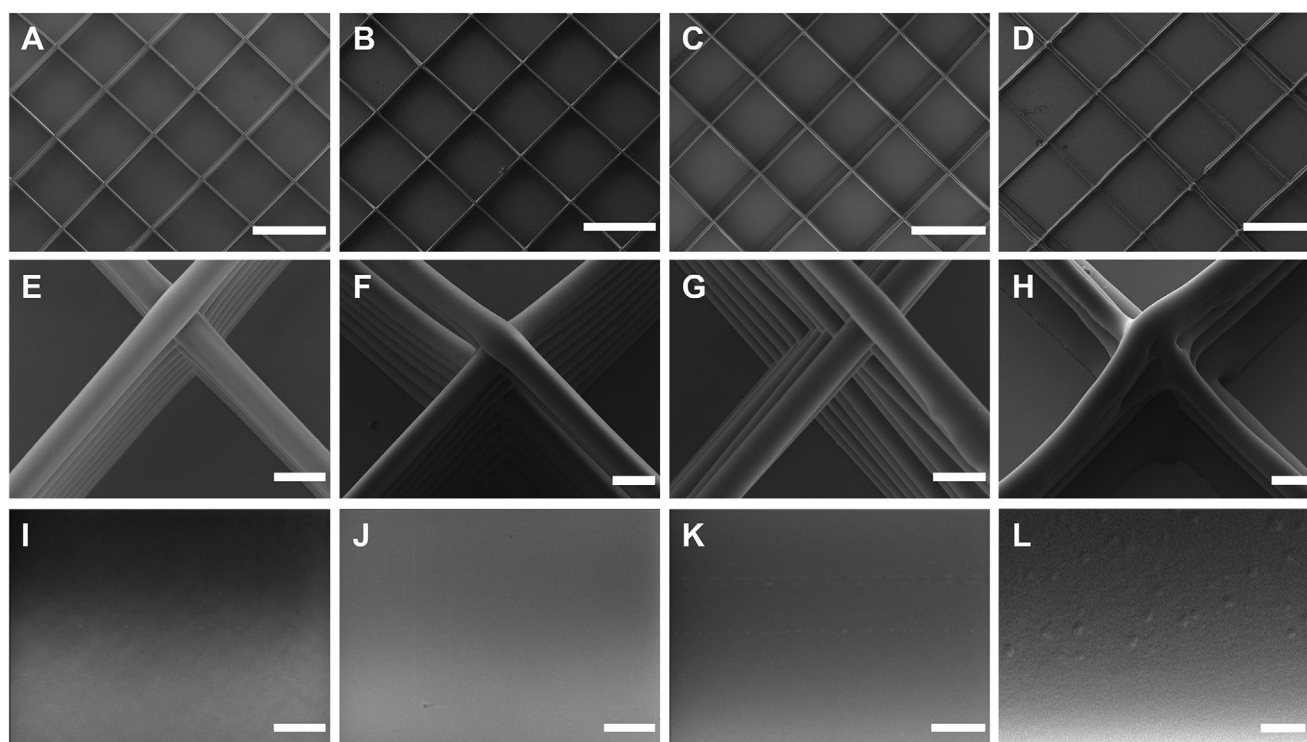


**Figure 4.** SEM images of copolymers **1** to **4**. A–D) Square-shaped MEW scaffolds with  $500\text{ }\mu\text{m}$  inter-fiber distance presenting the accurate and precise MEW fibers on top of each other for copolymer **1**, **2**, **3**, **4** respectively (scale bar:  $500\text{ }\mu\text{m}$ ). E–H) Well-stacked fibers on top of each other for copolymer **1**, **2**, **3**, **4** respectively (scale bar:  $20\text{ }\mu\text{m}$ ), and I–L) showing the smooth surface of the fibers for copolymer **1**, **2**, **3**, **4** respectively (scale bar:  $2\text{ }\mu\text{m}$ ).

square-shaped 10- and 20-layered constructs (Figure 4 and Figure S1, Supporting Information). As previously reported, copolymer **1** has an accurate and precise stacking behavior<sup>[16]</sup> while the copolymer **4** has lower shape fidelity compared to other copolymers at the same processing parameters. All other copolymers similarly stacked well; some defects begin occurring after 20 layers (Figure S1, Supporting Information). The copolymers also stacked upon each other with no observable deleterious interactions shown by Figure S2A,B, Supporting Information, wherein copolymer **3** was MEW upon a square design scaffold of copolymer **2**. A rationale to research physically crosslinked polymers

is that increased self-healing for improved fiber fusion, important for overall mechanics. The various swelling ratios or mechanical behaviors between different copolymers make this of interest for soft robotics. Using similar MEW processing conditions help when potentially switching between different copolymers while using a single nozzle — an approach already adopted within for extrusion direct writing.<sup>[38]</sup> For the future direction, the multi-material multi-nozzle 3D printing head could be used for MEW and in combination with the adjustable properties of segmented copolymers, very tiny voxelated soft matter can be generated.

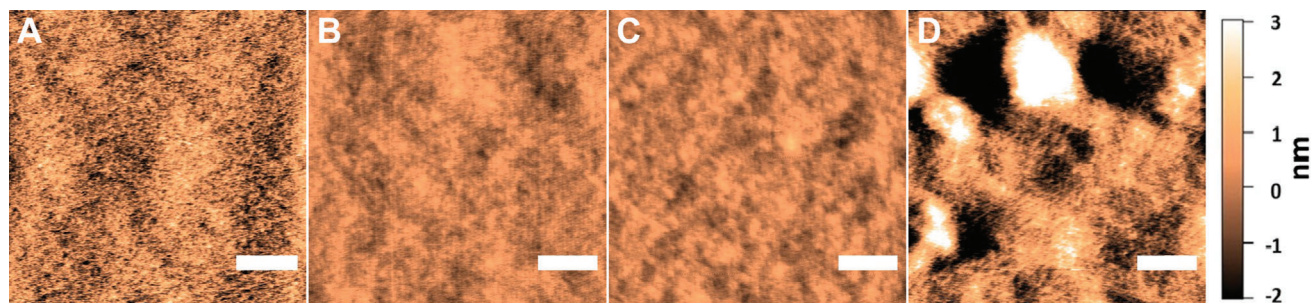


**Figure 5.** AFM height images of the copolymers. Copolymer A) 1, B) 2, C) 3, and D) 4 (scale bar: 200 nm). Height bar for all images shown on the right.

### 2.3. Topographical Analysis of Fiber Surfaces

The influence of different segment ratios of the  $(AB)_n$  and  $(ABAC)_n$  segmented copolymers on fiber topography was investigated using single layer MEW fibers with 20  $\mu\text{m}$  diameter for each copolymer. The fibers were printed between 800 and 2000  $\text{mm min}^{-1}$  with 3.0 kV, 1.0 bar, and 2.2 mm collector distance. The single layer, straight and continuous copolymer fibers with a uniform diameter were used in the study. The MEW fibers were extremely homogenous and exhibited a smooth fiber surface for all the copolymers as seen by scanning electron microscopy (SEM) (Figure 4I–L). Compared to other polymers investigated for MEW,<sup>[10,39]</sup> the smoothness and roughness of the fiber surface are notable difference. Often, morphological features such as spherulites<sup>[12]</sup> or striations<sup>[34]</sup> indicating flow-induced crystallization or microphase separation have been observed on the surface of MEW fibers, when semi-crystalline polymers were processed.

It is well-known that the chemical structure, average molecular weight, polarity, and volume fraction of the different segments strongly influence the morphology of a copolymer.<sup>[40,41]</sup> Therefore, atomic force microscopy (AFM) was used to investigate surface properties for the four different copolymers. AFM analysis suggests that the ratio between the different copolymer components influences the topography of the fiber surface (Figure 5). In particular, copolymer 4 fibers showed a rougher surface topography compared to the other copolymers, with a root mean square deviation of  $1.11 \pm 0.37$  nm. In comparison, surface roughness of copolymers 1, 2, and 3 were  $0.81 \pm 0.09$ ,  $0.44 \pm 0.04$ , and  $0.42 \pm 0.04$  nm, respectively. All surfaces have significantly different roughness values compared to each other, except for the comparably smooth surfaces of copolymers 2 and 3 ( $p < 0.005$ ). Those roughness values are smaller than MEW PCL.<sup>[39]</sup>

### 2.4. Inter-Layer Bonding Test

Bisurea segmented copolymers are also known for excellent bonding between single layers, meaning that physical crosslinks re-assemble after breaking.<sup>[17,41]</sup> At the MEW processing temperature, the bisurea segments disaggregate and reform during fiber formation upon cooling, acting as physical crosslinks throughout the polymer network. It is therefore expected that layers will strongly bond together at intersection points. The inter-layer bonding of 20  $\mu\text{m}$  MEW fibers from copolymers 1 to 3 are tested

with Y-shaped constructs (Figure 6A). The design of Y-shaped constructs is a fiber wall divided into two different walls to measure the strength of the bonds between the layers. The constructs are bent backward by 180° and peeled under uniaxial tensile loading condition shown in Figure 6B and C. Y-shaped constructs of copolymer 1 are shown in Figure 6D before the test and of copolymer 3 after testing in Figure 6E. It is ensured that the bonded portion of the Y-shaped constructs remains perpendicular to the applied force. Maximal force is calculated using force–displacement curve (Figure 6F,G). During printing, collector speeds are adjusted to achieve the same fiber diameters for all copolymers. However, such different collector speeds will affect the jet cooling rate and therefore inter-layer bonding. The collector speeds for Y-shaped construct are 800, 2000, and 2000  $\text{mm min}^{-1}$  for copolymer 1, 2, and 3, respectively. All three copolymers have significantly different maximum forces (Figure 6G), while copolymer 3 has the strongest inter-layer bonding with  $21 \pm 1$  mN. The results show that the inter-layer bonding was improved with the consisting of bisurea and PPO-PEG-PPO segments and the increasing printing speed.<sup>[42]</sup> The copolymer 4 could not be performed for this test because this copolymer shows an adhesive behavior on the printed surface and could not be removed without damage.

### 2.5. Contact Angle Measurement and Swelling Test

The surface hydrophilicity of the copolymers is examined on square-shaped MEW 10-layer scaffolds with 200  $\mu\text{m}$  inter-fiber distance. The scaffolds have  $109 \pm 20^\circ$ ,  $107 \pm 13^\circ$ , and  $98 \pm 5^\circ$  contact angles for copolymer 1, 2, and 3 respectively. Copolymer 4 immediately dissolved, when the water droplet is placed upon it.

The swelling behavior of the MEW scaffolds is examined by measuring the difference of the fiber width of 1-layer scaffolds and the area of 10-layer scaffolds, both with 500  $\mu\text{m}$  inter-fiber distance, between in dry state and after the exposure to water for 3 h. The fibers show a rapid swelling due to their small diameters. The maximum swelling is reached immediately after the scaffolds were exposed to water (Figure S3, Supporting Information). As expected, the degree of swelling increases with the hydrophilicity of the copolymer from 1 to 4. Due to its hydrophobicity, copolymer 1 shows no swelling behavior. Swelling is investigated for copolymer 2 with 39% while copolymer 3 shows a swelling of 42% on fiber diameter; 3% and 22% swelling is observed on 10-layer scaffold areas for copolymer 2 and 3, respectively.

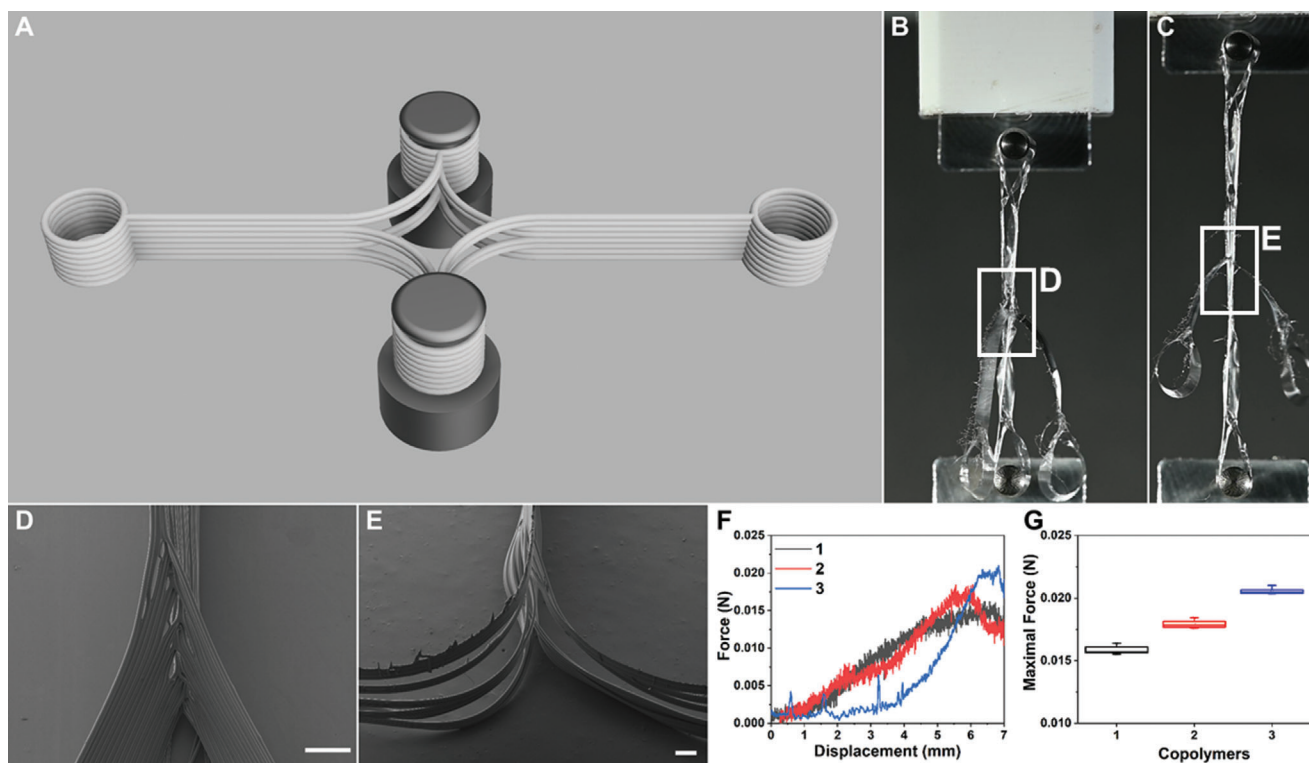


**Figure 6.** The inter-layer bonding behavior of the copolymers at crossover junctions. A) Rendered schematic of the test setup with two samples on metal pins. Inter-layer bonding testing setup B) before starting the test and C) during the test for copolymer 3. D) SEM pictures at crossover junction of copolymer 1 before the test and E) copolymer 3 after the test (scale bar: 200  $\mu\text{m}$ ). F) Force displacement and G) the average maximal force plot of the copolymers 1, 2, and 3.

## 2.6. In Vitro Cytocompatibility

Cytotoxicity of copolymers 1, 2, 3, and 4 is verified by elute test with L929 mouse murine fibroblast cells, as shown in Figure 7. Tissue culture polystyrene (PS) is used as a negative control and normalization for cellular activity, while poly(vinyl chloride) (PVC) is the positive control. The results of dsDNA amounts (Figure 7A), metabolic activity (Figure 7B), and metabolic activity per cells (Figure 7C) were normalized to negative control. Copolymers 1, 2, and 3 are non-cytotoxic. However, the cytotoxicity of copolymer 4 is depending on the concentration, thus, the copolymer displayed cytotoxicity in the range of 50–100%. The cytotoxicity of copolymer 4 is attributed to the PPO-PEG-PPO segments, which behave as a surfactant to the cell membrane.<sup>[43]</sup>

Live/Dead staining is performed with L929 cells on MEW scaffolds (Figure 7D–I) and cell viability is over 80% for copolymer 1, 2, and 3 at day 4. The attachment and proliferation, as well as metabolic activity of L929 cells on the MEW scaffolds, are determined via dsDNA content and metabolic cell activity at days 1 and 4 (Figure S4, Supporting Information). The results of PicoGreen assay indicate that dsDNA amounts are increased at day 4 compared to day 1 (Figure S4B, Supporting Information). However, the cell attachment is lower on copolymer 3 at day 1 compared to copolymer 1 and 2 due to the bioinert nature of PPO-PEG-PPO segments. Also, there is significantly less adhesion on the copolymer 3 scaffold compared to copolymer 1 and 2 at day 4.

The metabolic cell activity on MEW scaffolds is increased at day 4 except for copolymer 3 (Figure S4A, Supporting Information). Copolymer 4 is not investigated due to its immediate dissolution.

## 3. Conclusion

In conclusion,  $(\text{AB})_n$  and  $(\text{ABAC})_n$  segmented copolymers are well compatible with MEW at similar processing conditions. Smooth, well-formed fibers could be formed across different chemical compositions that ranged from hydrophobic through to hydrophilic. The fiber deposition can be well-controlled, enabling the fabrication of complex and layer-by-layer structures. When in contact with cells, the scaffolds either supported adhesion or dissolved without cytotoxic products at lower concentrations indicating that this class of copolymers has broad physical properties. There are several specialized areas such as capillary origami, microfluidic, flexible electronic device, soft network composites, sacrificial materials where these copolymers could have utility due to their unique surface properties, transparency, and adjustable hydrophilicity.

## 4. Experimental Section

**Materials:** The  $(\text{AB})_n$  and  $(\text{ABAC})_n$  segmented copolymers (Figure 1) were synthesized according to the previous work.<sup>[16,17,33]</sup> Copolymer 1 is a hydrophobic  $(\text{AB})_n$  segmented copolymer made of bisurea segments

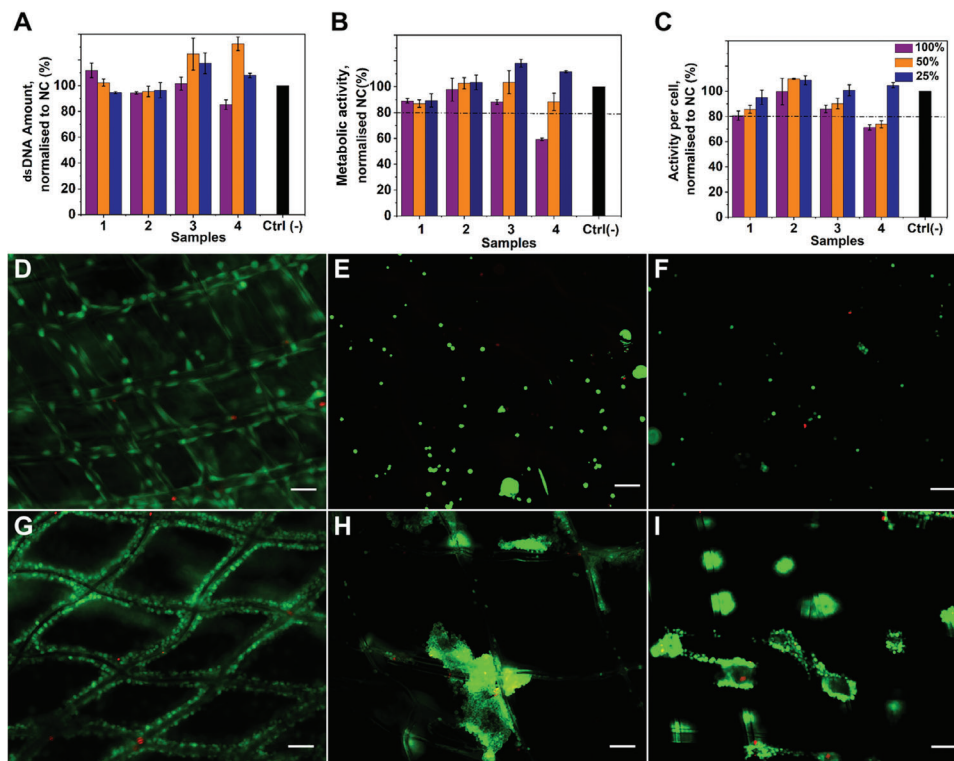


**Figure 7.** Cytotoxicity tests of copolymer films using L929 murine fibroblasts A–C) and viability of L929 murine fibroblast cells on MEW copolymers D–I). A) dsDNA amounts, B) metabolic activity, and C) metabolic activity per cell determined via eluate testing using PS and PVC as controls. Live/Dead staining (alive cells: green; dead cells: red) of attached L929 cells to MEW copolymers D–F) copolymer 1, 2, and 3 at day 1, G–I) at day 4, respectively. The cell attachment is lower with the present of the PPO-PEG-PPO segments (scale bar: 100  $\mu\text{m}$  at (E–I), 50  $\mu\text{m}$  at (D)).

and PDMS segments. Copolymers 2 and 3 are amphiphilic  $(\text{ABAC})_n$  segmented copolymers consisting of bisurea segments, hydrophobic PDMS segments, and hydrophilic PPO-PEG-PPO segments. The ratios between bisurea, PDMS, and PPO-PEG-PPO segments are 13:80:7 wt.% for copolymer 2 and 15:53:32 wt.% for copolymer 3. Copolymer 4 is a hydrophilic  $(\text{AB})_n$  segmented copolymer and has bisurea segments and PPO-PEG-PPO segments.

**Rheology:** Oscillatory shear rheology experiments of the copolymers were conducted using a Kinexus lab<sup>+</sup> rheometer (Malvern Panalytical) at a cooling rate of 2 K  $\text{min}^{-1}$  and a frequency of 1 Hz. Samples with a thickness around 1 mm were investigated in a 25 mm plate-plate geometry. First cooling cycle was recorded, whereas melting the sample in the rheometer was considered as first heating.

**MEW Device and Printing Parameters:** All experiments were performed with a custom-built MEW printer as previously described<sup>[17]</sup> and syringes pressurized with  $\text{N}_2$  and regulated using a pressure gauge (FESTO, Berkhelm, Germany). Inside the MEW head, a 26-gauge nozzle with the length of 5.4 or 7 mm (Unimed S.A., Lausanne, Switzerland) and a glass syringe (FORTUNA<sup>®</sup> Optima, 3 mL, Poulten & Graf GmbH, Wertheim, Germany) with the copolymer was heated by three ceramic electric heaters (Bach RS, Germany). The x-y movement of the collector was controlled by linear stages and operated by G-code. All MEW constructs were printed at an ambient temperature of  $21.5 \pm 1.5$  °C and relative humidity of  $35 \pm 2\%$ . Furthermore, all copolymers were processed at 100 °C and printability assessed using collector speeds ranging from 500 to 2800  $\text{mm min}^{-1}$  for 0.5 to 1.0 bar. The scaffold printing ultimately was performed on between 800 and 2000  $\text{mm min}^{-1}$  at 1.0 bar.

**Imaging:** The average fiber diameters were measured by using a tabletop SEM (TM3030, Hitachi High-Technologies Corporation, Mannheim, Germany) and a crossbeam 340 SEM equipped with GEMINI e-Beam column (Carl Zeiss Microscopy GmbH) with all samples imaged after platinum coating (Leica EM ACE600, Wetzlar, Germany). Video was recorded

using a Nikon Z6 digital camera with Nikon ED 200 mm lens. Furthermore, the SEM FEI Quanta FEG 250 (Thermo Fisher Scientific) was used for imaging the surface of the constructs. The untreated constructs were placed in the sample chamber of the FEI Quanta FEG 250, and the measurements were conducted in the low vacuum mode (water pressure of 40 Pa in the sample chamber).

**Atomic Force Microscopy (AFM):** AFM imaging was performed in air on a Molecular Force Probe (MFP) 3D system (Asylum Research, Oxford Instruments). Samples were scanned at  $2.5 \mu\text{m s}^{-1}$  in amplitude modulation mode using AC240 AFM probes with nominal resonance frequency of  $\approx 70$  kHz and spring constant of  $2 \text{ N m}^{-1}$ . Images were recorded at a resolution of  $1.95 \text{ nm pixel}^{-1}$ . Surface roughness values are given as averages from 8 to 14 different surface areas of  $250 \text{ nm} \times 250 \text{ nm}$  in at least two  $1 \mu\text{m} \times 1 \mu\text{m}$  images from independent fiber positions per sample and were measured as root mean square height variations using the MFP software (Asylum Research, Oxford Instruments).

**Contact Angle Measurement and Swelling Tests:** For the surface wettability test, MEW scaffolds with 10 layers with 200  $\mu\text{m}$  inter-fiber distance were used. The measurement was performed with deionized water using a static contact angle measurement instrument (Contact Angle System OCA20).

For the swelling experiment, a 1-layer and a 10-layer MEW scaffold with 500  $\mu\text{m}$  inter-fiber distance from every copolymer was exposed to deionized water at ambient conditions. The swelling was monitored and recorded by microscope (Nikon Dualphot 300). Pictures were taken for 3 h with a magnification at 10x. The fiber diameter and scaffold size change were determined by using ImageJ.

**Inter-Layer Bonding Test:** The Y-shaped constructs and mechanical setup allowed to test fiber bonding between layers shown in Figure 6A. Additional G-codes are provided in Supporting Information. The inter-layer bonding was measured with an ElectroForce 5500 test instrument (TA Instruments, USA) using a 250 g load cell, previously described.<sup>[44]</sup>

**Eluate and Direct Cell Cytotoxicity Testing:** Eluate tests were performed according to ISO 10 993-5 applying L929 (ATCC, Rockville, USA) cells. Copolymer films were incubated in cell culture media consisting of Dulbecco's modified Eagle's medium, GlutaMax, 1%, 1 m HEPES, 1% penicillin–streptomycin, and 10% FCS. Cytotoxic PVC platelets were used as a positive control. Elution medium without any incubated material served as a negative control while eluates prepared by material incubation for 48 h at 37 °C. Then, suspended sediments were centrifuged and the supernatant was referred to 100% eluate. Both 50% and 25% eluates were prepared by dilution with fresh cell culture medium. WST-1 and PicoGreen assays were performed to determine metabolic L929 cell activity and DNA amount, respectively after 2 days of incubation. All samples were tested at least in triplicates.

Cell adhesion experiments were performed with L929 cells, where a total of 500 000 cells were seeded on MEW 10-layer scaffolds with 500 or 250 µm inter-fiber distance. Live dead staining, PicoGreen, and WST-1 assays were performed on day 1 and 4 according to manufacturer's instruction.

**Statistics:** One-way analysis of variance was performed for statistical analysis. Statistical significance is defined as  $p < 0.05$ .

## Supporting Information

Supporting Information is available from the Wiley Online Library or from the author.

## Acknowledgements

The technical assistance of Philipp Stahlhut and Judith Friedlein for SEM imaging, Dr. Carina Blum for proof reading, Dr. Andrei Hrynevich for G-code generation, Andreas Züge for video recording, and Ievgenii Liashenko for video editing is highly appreciated. The authors thank Dr. Reiner Giesa for the help with rheological measurements and discussion. The project was financed by the Deutsche Forschungsgemeinschaft (DFG, German Research Foundation)—Project number 326998133—TRR 225 (sub-project A04). The DFG State Major Instrumentation Program (INST 105022/58-1 FUGG) funded the Zeiss Crossbeam CB 340 SEM used in this study.

Open access funding enabled and organized by Projekt DEAL.

## Conflict of Interest

The authors declare no conflict of interest.

## Data Availability Statement

Data available on request from the authors

## Keywords

3D printing, additive manufacturing, electrohydrodynamics, melt electrowriting

Received: July 14, 2021  
Revised: September 13, 2021  
Published online: October 17, 2021

- [1] A. Georgopoulou, L. Egloff, B. Vanderborght, F. Clemens, *Actuators* **2021**, 10, 102.  
[2] Z. Zhu, H. S. Park, M. C. Mcalpine, *Sci. Adv.* **2020**, 6, eaba5575.

- [3] A. Youssef, S. J. Hollister, P. D. Dalton, *Biofabrication* **2017**, 9, 012002.  
[4] D. W. Hutmacher, *Biomaterials* **2000**, 21, 2529.  
[5] T. D. Ngo, A. Kashani, G. Imbalzano, K. T. Q. Nguyen, D. Hui, *Composites, Part B* **2018**, 143, 172.  
[6] P. D. Dalton, *Curr. Opin. Biomed. Eng.* **2017**, 2, 49.  
[7] T. M. Robinson, D. W. Hutmacher, P. D. Dalton, *Adv. Funct. Mater.* **2019**, 29, 1904664.  
[8] G. Hochleitner, T. Jüngst, T. D. Brown, K. Hahn, C. Moseke, F. Jakob, P. D. Dalton, J. Groll, *Biofabrication* **2015**, 7, 035002.  
[9] E. C. L. Bolle, D. Nicdao, P. D. Dalton, T. R. Dargaville, In *Computer-Aided Tissue Engineering: Methods and Protocols*, (Eds.: A. Rainer, L. Moroni), Springer, New York, **2021**, pp. 111–124.  
[10] J. C. Kade, P. D. Dalton, *Adv. Healthcare Mater.* **2021**, 10, e2001232.  
[11] S. Florczak, T. Lorson, T. Zheng, M. Mrlik, D. W. Hutmacher, M. J. Higgins, R. Luxenhofer, P. D. Dalton, *Polym. Int.* **2019**, 68, 735.  
[12] J. N. Haigh, T. R. Dargaville, P. D. Dalton, *Mater. Sci. Eng., C* **2017**, 77, 883.  
[13] F. Chen, G. Hochleitner, T. Woodfield, J. Groll, P. D. Dalton, B. G. Amsden, *Biomacromolecules* **2016**, 17, 208.  
[14] R. S. Diaz, J. - R. Park, L. L. Rodrigues, P. D. Dalton, E. M. De-Juan-Pardo, T. R. Dargaville, *Adv. Mater. Tech.* **2021**, 2100508.  
[15] D. Nahm, F. Weigl, N. Schaefer, A. Sancho, A. Frank, J. Groll, C. Villmann, H. - W. Schmidt, P. D. Dalton, R. Luxenhofer, *Mater. Horiz.* **2020**, 7, 928.  
[16] G. Hochleitner, E. Fürsattel, R. Giesa, J. Groll, H. - W. Schmidt, P. D. Dalton, *Macromol. Rapid Commun.* **2018**, 39, 1800055.  
[17] J. Mechau, A. Frank, E. Bakirci, S. Gumbel, T. Jungst, R. Giesa, J. Groll, P. D. Dalton, H. - W. Schmidt, *Macromol. Chem. Phys.* **2021**, 222, 2170001.  
[18] B. D. Ratner, S. J. Bryant, *Annu. Rev. Biomed. Eng.* **2004**, 6, 41.  
[19] A. S. Hoffman, *Adv. Drug Delivery Rev.* **2002**, 54, 3.  
[20] W. Hu, S. Lu, Z. Zhang, L. Zhu, Y. Wen, T. Zhang, Z. Ji, *Biomater. Sci.* **2019**, 7, 1323.  
[21] M. D. Swartzlander, C. A. Barnes, A. K. Blakney, J. L. Kaar, T. R. Kyriakides, S. J. Bryant, *Biomaterials* **2015**, 41, 26.  
[22] J. S. Miller, K. R. Stevens, M. T. Yang, B. M. Baker, D.-H. T. Nguyen, D. M. Cohen, E. Toro, A. A. Chen, P. A. Galie, X. Yu, R. Chaturvedi, S. N. Bhatia, C. S. Chen, *Nat. Mater.* **2012**, 11, 768.  
[23] B. Grigoryan, S. J. Paulsen, D. C. Corbett, D. W. Sazer, C. L. Fortin, A. J. Zaita, P. T. Greenfield, N. J. Calafat, J. P. Gounley, A. H. Ta, F. Johansson, A. Randles, J. E. Rosenkrantz, J. D. Louis-Rosenberg, P. A. Galie, K. R. Stevens, J. S. Miller, *Science* **2019**, 364, 458.  
[24] T. Lorson, S. Jaksch, M. M. Lübtow, T. Jüngst, J. Groll, T. Lühmann, R. Luxenhofer, *Biomacromolecules* **2017**, 18, 2161.  
[25] D. Williams, In *Tissue Engineering*, Academic Press, Burlington, **2008**, pp. 255–278.  
[26] J. He, X. Zhao, J. Chang, D. Li, *Small* **2017**, 13, 1702626.  
[27] M. Castilho, R. Levato, P. N. Bernal, M. De Ruijter, C. Y. Sheng, J. Van Duijn, S. Piluso, K. Ito, J. Malda, *Biomacromolecules* **2021**, 22, 855.  
[28] G. M. Pawar, M. Koenigs, Z. Fahimi, M. Cox, I. K. Voets, H. M. Wyss, R. P. Sijbesma, *Biomacromolecules* **2012**, 13, 3966.  
[29] Q. Chen, X. Mei, Z. Shen, D. Wu, Y. Zhao, L. Wang, X. Chen, G. He, Z. Yu, K. Fang, D. Sun, *Opt. Lett.* **2017**, 42, 5106.  
[30] F. Kotz, P. Risch, K. Arnold, S. Sevim, J. Puigmartí-Luis, A. Quick, M. Thiel, A. Hrynevich, P. D. Dalton, D. Helmer, *Nat. Commun.* **2019**, 10, 1.  
[31] K. Koenig, K. Beukenberg, F. Langensiepen, G. Seide, *Biomater. Res.* **2019**, 23, 1.  
[32] O. Bas, E. M. De-Juan-Pardo, C. Meinert, D. D'angella, J. G. Baldwin, L. J. Bray, R. M. Wellard, S. Kollmannsberger, E. Rank, C. Werner, T. J. Klein, I. Catelas, D. W. Hutmacher, *Biofabrication* **2017**, 9, 025014.



- [33] E. M. Fürsattel, *Extrusion-Based Melt Processing of (AB)<sub>n</sub> Segmented Poly(urea-siloxane)s and their Modification towards Amphiphilic Hydrogels*, University of Bayreuth, Bayreuth, Germany **2021**.
- [34] G. Hochleitner, A. Youssef, A. Hrynevich, J. N. Haigh, T. Jungst, J. Groll, P. D. Dalton, *BioNanomaterials* **2016**, *17*, 159.
- [35] A. Hrynevich, I. Liashenko, P. D. Dalton, *Adv. Mater. Technol.* **2020**, *5*, 2000772.
- [36] J. Kim, E. Bakirci, K. L. O'neill, A. Hrynevich, P. D. Dalton, *Macromol. Mater. Eng.* **2021**, *306*, 2000685.
- [37] A. Hrynevich, B. Ş. Elçi, J. N. Haigh, R. McMaster, A. Youssef, C. Blum, T. Blunk, G. Hochleitner, J. Groll, P. D. Dalton, *Small* **2018**, *14*, e1800232.
- [38] M. A. Skylar-Scott, J. Mueller, C. W. Visser, J. A. Lewis, *Nature* **2019**, *575*, 330.
- [39] C. Blum, J. Weichhold, G. Hochleitner, V. Stepanenko, F. Würthner, J. Groll, T. Jungst, *3D Print. Addit. Manuf.* **2021**. <http://doi.org/10.1089/3dp.2020.0290>.
- [40] S. Sami, E. Yildirim, M. Yurtsever, E. Yurtsever, E. Yilgor, I. Yilgor, G. L. Wilkes, *Polymer* **2014**, *55*, 4563.
- [41] N. Candau, G. Stoclet, J. - F. Tahon, A. Demongeot, E. Yilgor, I. Yilgor, Y. Z. Menciloglu, O. Oguz, *Polymer* **2021**, *223*, 123708.
- [42] E. Bakirci, N. Schaefer, O. Dahri, A. Hrynevich, P. Strissel, R. Strick, P. D. Dalton, C. Villmann, *Adv. Biosyst.* **2020**, *4*, 2000077.
- [43] L. Castan, C. José Da Silva, E. Ferreira Molina, R. Alves Dos Santos, *J. Biomed. Mater. Res., Part B* **2018**, *106*, 742.
- [44] I. Liashenko, A. Hrynevich, P. D. Dalton, *Adv. Mater.* **2020**, *32*, 2001874.